A measurement method of absolute hydrogen atom density in plasmas by (2+1)-photon laser-induced fluorescence spectroscopy

K. Sasaki,[a] M. Nakamoto, and K. Kadota
Department of Electronics, Nagoya University, Nagoya 464-8603, Japan

(Received 26 September 2000; accepted for publication 22 February 2001)

A technique of $(2+1)$-photon laser-induced fluorescence (LIF) spectroscopy has been developed for measuring hydrogen atom density in plasmas. In this method, the following two-step excitation scheme is employed to excite ground-state H atoms to the $4p$ state. In the first step, H atoms at the ground $(1s)$ state are excited to the $2s$ state by two photons at a wavelength of 243 nm. Subsequently, the $2s$ state is excited to the $4p$ state by the third photon at 486 nm in the second step. Fluorescence emission at 486 nm ($4p \rightarrow 2s$, H_β line) is detected to determine the H atom density at the ground state. Since the wavelength used in the first-step excitation is the half of the wavelength used in the second-step excitation, one tunable laser with a system for second harmonic generation can be utilized in the measurement. The absolute density was evaluated by comparing the intensity of LIF emission from H with that from Xe at a known gas pressure. The present method is suitable for diagnostics of reactive plasmas since optical dissociation of molecules and radicals can be avoided because of the low photon energy of the laser radiation. © *2001 American Institute of Physics.* [DOI: 10.1063/1.1367356]

I. INTRODUCTION

Measurement of absolute hydrogen atom density is an important issue in studies of various plasmas. In nuclear fusion research, it is known that hydrogen atoms in the scrapeoff layer and diverter area have significant influence on the confinement of high-temperature core plasmas. In material processing using low-temperature reactive plasmas, H atoms play principal roles in gas-phase and surface reactions. However, determination of absolute H atom density in plasmas is not an easy task. In addition, many plasmas require measurement techniques with temporal and spatial resolutions.

Titration,[1] actinometry,[2,3] and vacuum ultraviolet absorption spectroscopy[4,5] are applicable to the measurement of H atom density. However, these methods are lacking in spatial resolution. Although titration using NO_2 can yield the absolute H atom density, the injection of NO_2 may seriously disturb the plasma. Actinometry (optical emission spectroscopy) is a simple technique, but the determination of the absolute density is difficult. In addition, since the result of actinometry is a sensitive function of the distribution of electron energy in the plasma, the reliability of actinometry is questionable especially in low-pressure, high-density plasmas.[6] Vacuum ultraviolet absorption spectroscopy using the Lyman α transition can be used to evaluate the absolute H atom density. However, the reliability of vacuum ultraviolet absorption spectroscopy is lowered by distorted spectral distribution of the probe emission.[4,5]

Laser-induced fluorescence (LIF) spectroscopy is a method for measuring the H atom density in plasmas with temporal and spatial resolutions.[7,8] In conventional LIF for the detection of the H atom, a laser beam at a wavelength of 205 nm is launched into plasma to excite H atoms at the ground state ($1s$ state) to the $n=3$ state.[4,9] Fluorescence emission from the $n=3$ to $n=2$ states (H_α emission) is observed. In the present work, we have developed another LIF technique using a multiple-photon excitation scheme. The present method employs two wavelengths at 243 and 486 nm, which are yielded from one tunable laser. This method is suitable for the diagnostics of reactive plasmas since optical dissociation of molecules and radicals can be avoided because of the low photon energy of the laser beam.

An issue in LIF is the evaluation of the absolute density from the fluorescence signal. In the present work, we have developed a calibration method to determine the absolute H atom density. The calibration method is based on a comparison of the intensity of fluorescence emission from H with that from Xe at a known gas pressure.[10] The excitation and emission processes in H and Xe are modeled by rate equations. The absolute H atom density is evaluated from the emission intensity ratio measured experimentally, by referring to the results of rate equation analysis.

II. SCHEME OF (2+1)-PHOTON LIF

Figure 1 shows the partial energy level diagram of the H atom. In the present LIF spectroscopy, H atoms at the ground $(1s)$ state are excited to the $4p$ state by the following two-step excitation scheme, and fluorescence emission at a wavelength of 486 nm ($4p \rightarrow 2s$, H_β line) is observed. In the first step of the excitation, ground-state H atoms are excited to the $2s$ state by two photons at 243 nm. Subsequently, the $2s$ state is excited to the $4p$ state by the third photon at 486 nm in the second step. Since the wavelength used in the first-step excitation is the half of the wavelength used in the second-step excitation, one tunable laser with a system for second harmonic generation can be used in the $(2+1)$-photon exci-

[a]Author to whom correspondence should be addressed; electronic mail: sasaki@nuee.nagoya-u.ac.jp

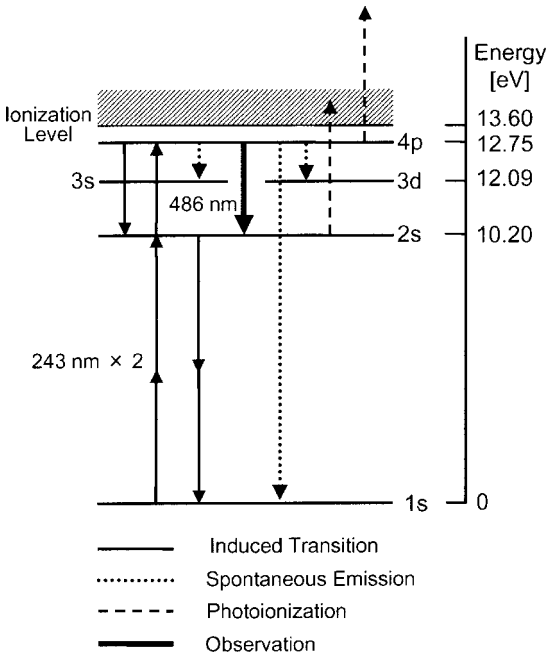

FIG. 1. Transitions considered in the rate equation model for H.

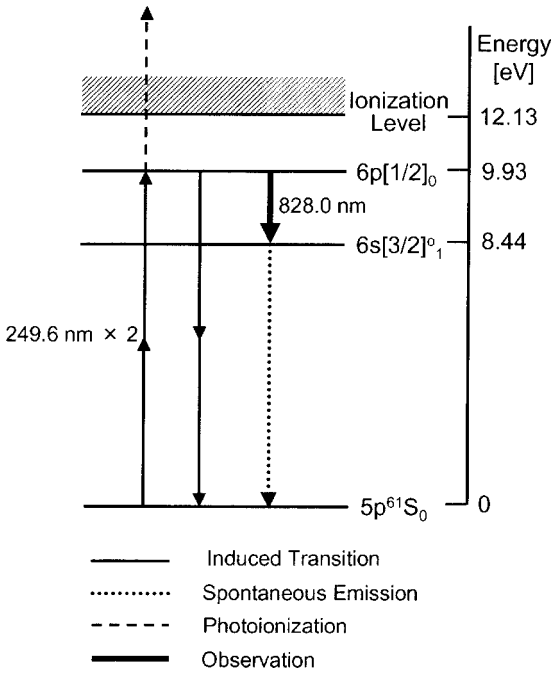

FIG. 2. Transitions considered in the rate equation model for Xe.

tation. Since the transition energy between the $1s$ and $2s$ states is resonant with the two-photon absorption at 243 nm, the efficiency of the $(2+1)$-photon excitation is much greater than that of the simple (nonresonant) three-photon excitation.

This $(2+1)$-photon excitation scheme was proposed originally by Gathen *et al.*[11] There are two major advantages in the $(2+1)$-photon excitation scheme, in comparison with the conventional two-photon LIF scheme employing a laser at a wavelength of 205 nm. One is easy generation of ultraviolet laser radiation for the excitation. The laser radiation at 205 nm is generated from a laser radiation at 615 nm by a two-step wavelength conversion technique using KDP and BBO crystals. Contrary to this, the laser radiation at 243 nm can be obtained from a laser radiation at 486 nm by simple second harmonic generation. The other advantage is the low photon energy of the laser radiation at 243 nm. In the diagnostics of reactive plasmas, the low photon energy is important to avoid optical dissociation of molecules and radicals. Miyazaki *et al.* have shown significant optical dissociation of SiH_4 by the laser radiation at 205 nm.[12] To avoid the optical dissociation, they have developed a system using two tunable lasers; one is used for the excitation from the $1s$ to $2s$ states and the other is used for the excitation from the $2s$ to $3p$ states.[13] Contrary to the method employing two tunable lasers, one tunable laser can be used for the present $(2+1)$-photon LIF scheme, which is a merit of the present excitation scheme.

III. METHOD FOR ABSOLUTE DENSITY CALIBRATION

A. Principles of calibration

The calibration method to determine the absolute H atom density is based on a comparison of the LIF emission from H with that from Xe at a known gas pressure. The use of Xe as a reference gas has been proposed by Goehlich *et al.*, and has been demonstrated in the determination of absolute O atom density measured by two-photon LIF.[10] Figure 2 shows the partial energy level diagram of Xe. In the LIF measurement for the absolute density calibration, ground-state ($5p^6\,{}^1S_0$ state) Xe atoms are excited to the $6p[1/2]_0$ state by two photons at 249.6 nm. Fluorescence emission at 828.0 nm ($6p[1/2]_0 \rightarrow 6s[3/2]_1^o$) is detected using the same optical system as that used in the LIF measurement for H atoms. Xe gas at a known pressure is filled in the same vacuum chamber as that used in plasma experiments. To determine the absolute H atom density from the emission intensity ratio, it is necessary to evaluate the excitation efficiency of Xe and H. Rate equation models were constructed to evaluate the production efficiency of the $6p[1/2]_0$ state of Xe and the $4s$ state of H. Induced transition, spontaneous emission, and photoionization processes illustrated in Figs. 1 and 2 are included in the rate equation models.

B. Rate equation model for H

The populations of the $1s$, $2s$, and $4p$ states of H are calculated by using rate equations that take into account induced transition, spontaneous emission, and photoionization processes of H. For the laser intensity at 486 nm used in the present experiment, complete saturation is expected for the excitation from $2s$ to $4p$. This is supported by the fact that the frequency of induced transition between $2s$ and $4p$ is evaluated to be much (approximately 10^3 times) higher than those of spontaneous emission and photoionization from the $4p$ state. Hence we can assume that the population distribution between the $2s$ and $4p$ states is equilibrated

$$N_{2s}/g_{2s} = N_{4p}/9_{4p}, \tag{1}$$

where N_i represents the reduced population of the ith state, which is normalized by the ground-state H atom density without the laser irradiation, n_{H}, such that $N_i = n_i/n_{\mathrm{H}}$. The

TABLE I. Various parameters used in the rate equation model for H.

Quantities	Values	Units	References
α_H	1.13×10^{-35}	m^4/W	12
σ_{pi}^{2s}	6.13×10^{-22}	m^2	13
σ_{pi}^{4p}	3.89×10^{-23}	m^2	13
A_{4p-1s}	6.82×10^{7}	s^{-1}	14
A_{4p-2s}	9.67×10^{6}	s^{-1}	14
A_{4p-3s}	3.07×10^{6}	s^{-1}	14
A_{4p-3d}	3.48×10^{5}	s^{-1}	14
$\sum_{i=1s,2s,3s,3d} A_{4p-i}$	8.09×10^{7}	s^{-1}	14

statistical weight of the ith state is denoted by g_i. The population of the $4p$ state is evaluated by solving rate equations which include two-photon absorption and stimulated emission between $1s$ and $2s$, photoionization from $2s$ and $4p$, and spontaneous emission from $4p$:

$$\frac{dN_{1s}}{dt} = -\frac{\alpha_H I_L^2}{h\nu_L} N_{1s} + \frac{g_{1s}}{g_{2s}} \frac{\alpha_H I_L^2}{h\nu_L} N_{2s} + A_{4p-1s} N_{4p}, \quad (2)$$

$$\frac{d(N_{2s}+N_{4p})}{dt} = \frac{\alpha_H I_L^2}{h\nu_L} N_{1s} - \left(\frac{g_{1s}}{g_{2s}} \frac{\alpha_H I_L^2}{h\nu_L} + \frac{\sigma_{pi}^{2s} I_L}{h\nu_L} \right) N_{2s} - \left(\frac{\sigma_{pi}^{4p} I_L}{h\nu_L} + \sum_{i=1s,3s,3d} A_{4p-i} \right) N_{4p}, \quad (3)$$

where $h\nu_L$ (J) and I_L (W/m^2) are the photon energy and the laser intensity at 243 nm, respectively, σ_{pi}^{i} (m^2) is the cross section for photoionization from the ith state at 243 nm, α_H (m^4/W) denotes the coefficient for two-photon absorption and stimulated emission between $1s$ and $2s$, and A_{4p-i} (s^{-1}) is the transition probability from the $4p$ to ith states. The collisional transition from the $2s$ to $2p$ states by electron impact is ignored since its collision frequency is much smaller than that of photoionization from $2s$. Photoionization by the laser beam at 486 nm is also ignored because of the weak laser intensity. Equations (1)–(3) are solved for an initial condition of $N_{1s}(0)=1$, $N_{2s}(0)=0$, and $N_{4p}(0)=0$ to evaluate the temporal variation of N_{4p}. A rectangular shape with a duration of 3.6 ns was assumed for the temporal variation of I_L. Various constants contained in the rate equations are found in the literature[14–16] as summarized in Table I.

C. Rate equation model for Xe

The populations of the $5p^6\,{}^1S_0$, $6p[1/2]_0$, and $6s[3/2]_1^o$ states are calculated by considering two-photon absorption and stimulated emission between $5p^6\,{}^1S_0$ and $6p[1/2]_0$, photoionization from $6p[1/2]_0$, and spontaneous emissions from $6p[1/2]_0$ and $6s[3/2]_1^o$. The rate equations are given by

$$\frac{dN_{5p}}{dt} = -\frac{\alpha_{Xe} I_L^2}{h\nu_L} N_{5p} + \frac{g_{5p}}{g_{6p}} \frac{\alpha_{Xe} I_L^2}{h\nu_L} N_{6p} + A_{6s-5p} N_{6s}, \quad (4)$$

$$\frac{dN_{6p}}{dt} = \frac{\alpha_{Xe} I_L^2}{h\nu_L} N_{5p} - \left(\frac{g_{5p}}{g_{6p}} \frac{\alpha_{Xe} I_L^2}{h\nu_L} + \frac{\sigma_{pi}^{6p} I_L}{h\nu_L} + A_{6p-6s} \right) N_{6p}, \quad (5)$$

TABLE II. Various parameters used in the rate equation model for Xe.

Quantities	Values	Units	References
α_{Xe}	3.40×10^{-35}	m^4/W	15
α_{pi}^{6p}	4.30×10^{-22}	m^2	15
A_{6p-6s}	3.33×10^{7}	s^{-1}	16
A_{6s-5p}	2.81×10^{8}	s^{-1}	17

$$\frac{dN_{6s}}{dt} = A_{6p-6s} N_{6p} - A_{6s-5p} N_{6s}, \quad (6)$$

where similar symbols to those in Eqs. (2) and (3) are used. The normalized population of the ith state of Xe is defined by $N_i = n_i / n_{Xe}$ with n_{Xe} being the density of Xe gas determined from the pressure. Various constants used in Eqs. (4)–(6) are summarized in Table II.[17–19]

In the absolute density calibration of O atom density carried out by Goehlich *et al.*,[10] the pump laser intensity was so weak that photoionization processes are negligible and the intensity of fluorescence emission was proportional to I_L^2. However, the weak pump laser intensity results in the low sensitivity of the measurement. In the present work, we used strong pump laser intensity to realize a sensitive detection limit, so that we considered photoionization processes in the rate equations.

D. Method of calibration

The intensities of fluorescence emissions from H and Xe, I_H and I_{Xe}, are proportional to the populations of the $4p$ and $6p[1/2]_0$ states, respectively. With a constant γ_λ representing the sensitivity of the detection system at a wavelength of λ, I_H and I_{Xe} are given by $I_H(t) = \gamma_{486} A_H N_H^*(t) n_H$ and $I_{Xe}(t) = \gamma_{828} A_{Xe} N_{Xe}^*(t) n_{Xe}$, where simplified notations $A_H = A_{4p-2s}$, $A_{Xe} = A_{6p-6s}$, $N_H^* = N_{4p}$, and $N_{Xe}^* = N_{6p}$ are used. Although the emission intensities have rapid temporal variations, their time integrals $\int_0^\infty I_H(t)dt$ and $\int_0^\infty I_{Xe}(t)dt$ are measured by using a boxcar integrator in the experiment. Therefore, we obtain

$$n_H = \frac{\gamma_{828}}{\gamma_{486}} \cdot \frac{A_{Xe}}{A_H} \cdot \frac{\int_0^\infty N_{Xe}^*(t)dt}{\int_0^\infty N_H^*(t)dt} \cdot \frac{\int_0^\infty I_H(t)dt}{\int_0^\infty I_{Xe}(t)dt} \cdot n_{Xe}. \quad (7)$$

The absolute H atom density is evaluated from the emission intensity ratio $\int_0^\infty I_{Xe}(t)dt / \int_0^\infty I_H(t)dt$ obtained experimentally and the population ratio $\int_0^\infty N_{Xe}^*(t)dt / \int_0^\infty N_H^*(t)dt$ determined by the rate equation analysis. The value of $\gamma_{828}/\gamma_{486}$ is measured experimentally using a tungsten standard lamp.

IV. EXPERIMENT

The present measurement method was examined in high-density hydrogen plasmas produced by helicon-wave discharges. The experimental apparatus is schematically shown in Fig. 3. The vacuum chamber was installed in a uniform magnetic field of 1 kG along the cylindrical axis of the vacuum chamber. It was composed of stainless-steel rectangular chambers (observation chambers) of $20\times20\times10$ cm and a Pyrex glass tube of 9 cm diameter. A quartz glass tube (discharge tube) of 3 cm diameter was attached to one of the observation chambers. A helical antenna was wound around

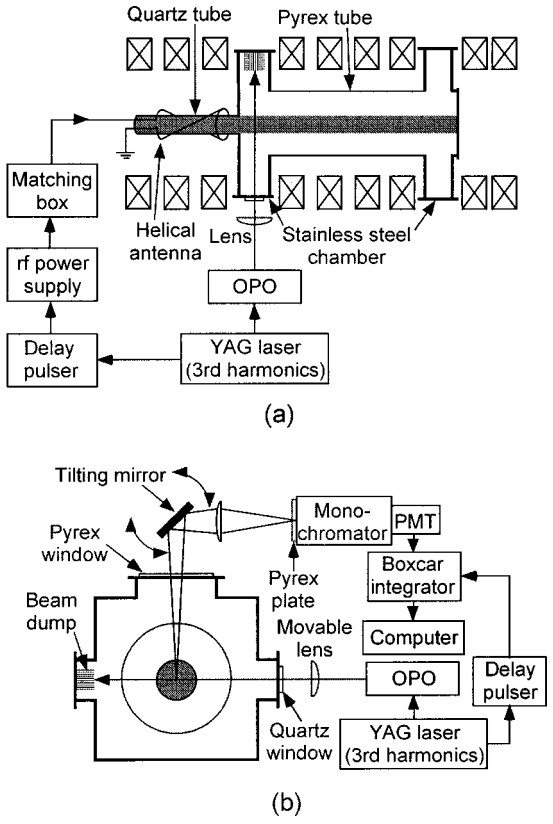

FIG. 3. Schematic of the experimental apparatus.

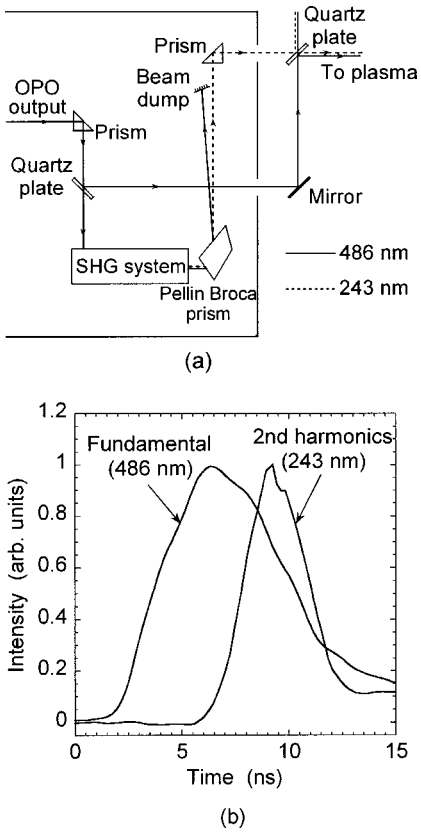

FIG. 4. Arrangement of the optical parametric oscillator (a) and the wave forms of laser pulses at wavelengths of 243 and 486 nm.

the discharge tube. Helicon-wave discharges were obtained by applying a rf power at 13.56 MHz to the helical antenna. The operating gas was pure H_2 at a flow rate of 10 ccm. Plasmas were produced in a pulsed mode with a repetition frequency of 10 Hz and a discharge duration of 10 ms. A high-density plasma column with a diameter of 3 cm was localized around the center of the vacuum chamber since the plasma was confined radially by the external magnetic field.

An optical parametric oscillator (OPO) (Spectra Physics MOPO-SLX) pumped by the third harmonic of a Nd:YAG laser (Spectra Physics GCR-230-HB) was used as the light source in the LIF measurement. The optical configuration of OPO was remodeled as shown in Fig. 4(a) in order to superpose the laser beam at 486 nm on the laser beam at 243 nm. The energies of the laser radiations at 243 and 486 nm were approximately 3 mJ and 30 μJ, respectively. The linewidth of the laser pulses was approximately 0.2 cm^{-1}. Considering the Doppler broadening of the transitions, both the excitations of $1s \rightarrow 2s$ and $2s \rightarrow 4p$ can be obtained by the laser pulses. The removal of a Pellin Broca prism is another method to superpose two laser beams. However, since the excitation from the $2s$ to $4p$ states is easily saturated for weak laser radiation, intense laser radiation at 486 nm does not contribute to the increase in the LIF emission intensity. Since the intense laser radiation at 486 nm resulted in strong stray light, we chose the optical configuration shown in Fig. 4(a). Figure 4(b) shows the wave forms of the laser pulses at 243 and 486 nm. As shown in the figure, the pulse duration (full width half maximum) of the laser pulses were 3.6 and 6.5 ns for 243 and 486 nm, respectively. Since the second harmonic (243 nm) had a longer path length than the fundamental radiation (486 nm), the arrival time of the laser pulse at 243 nm was slightly delayed from that at 486 nm. However, such a small delay was not a problem for the two-step excitation.

The OPO laser beams were focused into the plasma at the observation chamber of the upstream side through a quartz glass window. The focal length of the quartz lens was 40 cm. A beam dump was installed at the port of the opposite side to eliminate stray light. The distance between the laser beam and the end of the helical antenna was approximately 10 cm. The LIF emission was detected through an upper port using a monochromator and a photomultiplier tube. The width of the entrance slit of the monochromator was 1 mm, which corresponded to the spatial resolution of the measurement. The signal was averaged using a boxcar integrator and was recorded with a computer. The gate width of the boxcar integrator was 100 ns, which was much longer than the lifetimes of the excited states. In the present LIF scheme, both the laser radiations at 243 and 486 nm are the source of stray light, since the radiation at 243 nm goes into the photomultiplier tube via the second-order diffraction in the monochromator. In order to reduce the stray light at 243 nm, a Pyrex glass plate was used for the window of the upper port. In addition, another Pyrex glass plate was placed in front of the entrance slit of the monochromator. The tilting mirror and the lens for the incident laser beam were movable, in order to measure the spatial (radial) distribution of the H atom density along the path of the OPO laser beams. The scan of the

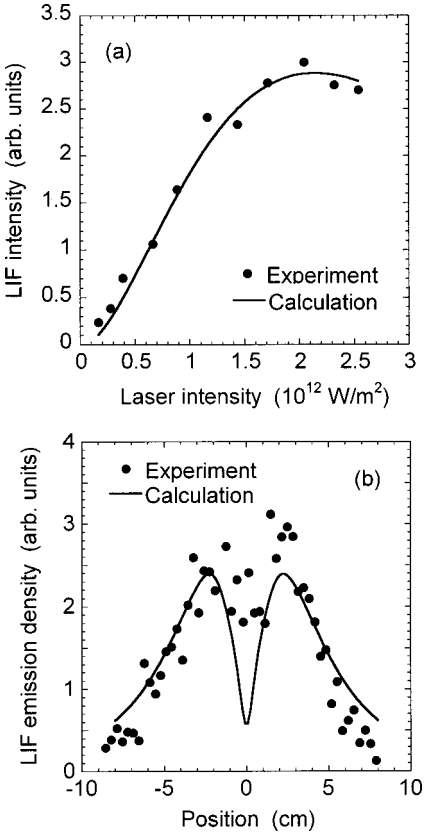

FIG. 5. Comparison between experimental results and rate equation analysis for Xe: (a) relation between the pump laser and LIF intensities, (b) LIF emission density as a function of the position along the path of the pump laser beam.

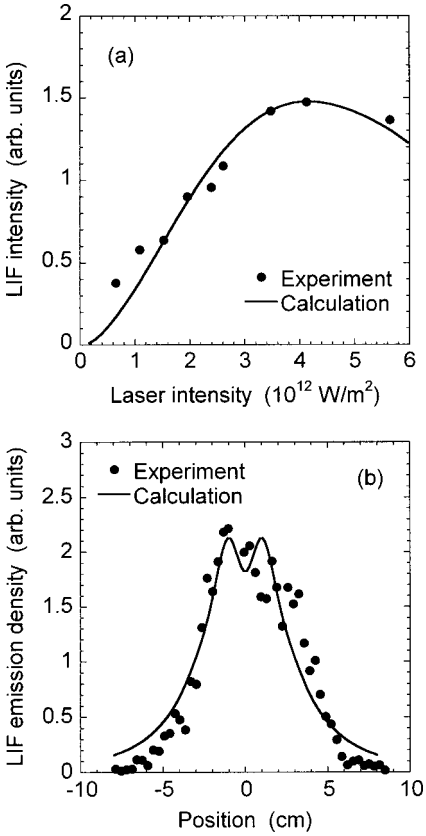

FIG. 6. Similar plots to those shown in Fig. 4 for the case of H.

tilting mirror was synchronized with the movement of the lens such that the observation position of the fluorescence emission coincided with the focus of the laser beam at 243 nm.

V. RESULTS AND DISCUSSION

A. Validity of the rate equation analysis

The intensity of the LIF emission was measured in Xe gas at a pressure of 7 mTorr as a function of the laser energy. The relation between the laser and LIF intensities is shown in Fig. 5(a), together with $\int_0^\infty N_{\mathrm{Xe}}^*(t)dt$ calculated from Eqs. (4)–(6). The saturation of $\int_0^\infty N_{\mathrm{Xe}}^*(t)dt$ for the laser intensity higher than 2×10^8 W/cm^2 is due to significant photoionization from the $6p[1/2]_0$ state. In this experiment, the focus of the laser beam at 249.6 nm was located at the center of the vacuum chamber, and the observation position was 2 cm away from the focus. We determined the intensity of the laser beam at the observation position by fitting the experimental curve to the calculated one. From the agreement between the experimental and calculated curves, the diameter of the laser beam at the observation position was evaluated to be 0.57 mm. By repeating the same measurements at different observation positions, we roughly estimated the distribution of the spot size of the laser beam as a function of the distance from the focus. As a result, the diameter of the laser beam at the focus was evaluated to be 0.35 mm.

Figure 5(b) shows the distribution of the LIF emission density along the path of the laser beam, when the focus was fixed at the center of the vacuum chamber. The distribution of $\int_0^\infty N_{\mathrm{Xe}}^*(t)dt$ obtained by the rate equation analysis is shown by the solid curve. The distribution of the pump laser intensity used in the rate equation analysis was calculated from the distribution of the spot size, which was estimated experimentally as described above. The LIF emission density was defined by the LIF intensity divided by the excitation volume. The excitation volume was calculated from the distribution of the spot size. As shown in Fig. 5(b), reasonable agreement between the experimental results and rate equation analysis was obtained, supporting the validity of the rate equation model for Xe [Eqs. (4)–(6)] used in the present work. The dip at the focus ($r=0$ cm) is due to the significant photoionization from the $6p[1/2]_0$ state.

The relation between the laser and LIF intensities is also examined in an H_2 plasma at an rf power of 0.5 kW and a pressure of 30 mTorr. Figure 6(a) shows the experimental relation between the laser and LIF intensities, together with $\int_0^\infty N_{\mathrm{Xe}}^*(t)dt$ calculated from Eqs. (1)–(3). The laser intensity was evaluated from the distribution of the spot size which was estimated by LIF experiments in Xe. As shown in Fig. 6(a), the experimental results agreed well with the rate equation analysis. Figure 6(b) shows the distribution of the LIF emission density along the path of the laser beam, when the focus was fixed at the center of the vacuum chamber. As will be described below, the radial distribution of the H atom density was uniform for an rf power of 500 W and an H_2 pressure of 30 mTorr. The distribution of $\int_0^\infty N_{\mathrm{Xe}}^*(t)dt$ ob-

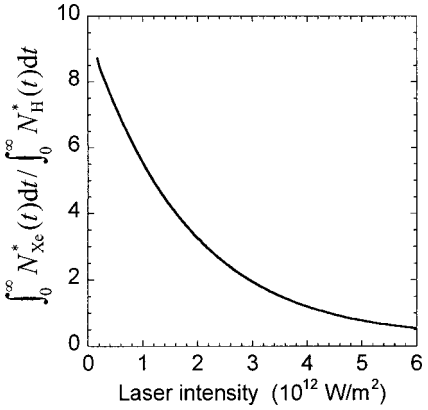

FIG. 7. Relationship between the laser intensity and the ratio of $\int_0^\infty N^*_{Xe}(t)dt/\int_0^\infty N^*_H(t)dt$ calculated by the rate equation model.

tained by the rate equation analysis is shown by the solid curve, where the pump laser intensity and the excitation volume were calculated from the distribution of the spot size estimated by LIF experiments in Xe. As shown in Fig. 6(b), the spatial distribution of the LIF emission density was also consistent with the rate equation analysis. Therefore, it is expected that the excitation and emission processes in H can be analyzed by Eqs. (1)–(3).

Figure 7 shows the relationship between the laser intensity and the ratio of $\int_0^\infty N^*_{Xe}(t)dt/\int_0^\infty N^*_{Xe}(t)dt$ calculated by the rate equation analysis. From the laser intensity dependences of $\int_0^\infty N^*_{Xe}(t)dt$ and $\int_0^\infty N^*_{Xe}(t)dt$ shown in Figs. 5(a) and 6(a), the ratio becomes a decreasing function of the laser intensity. One can evaluate the absolute H atom density from Eq. (7) by using the value of $\int_0^\infty N^*_{Xe}(t)dt/\int_0^\infty N^*_{Xe}(t)dt$ at the laser intensity used in the experiment.

B. Absolute H atom density

As has been described above, the results of the rate equation analysis were fairly consistent with the experimental results, indicating the validity of the rate equation models for the excitation and emission processes in H and Xe. On the basis of the agreement between the experimental results and the rate equation analysis, we evaluated the absolute H atom density in plasmas using Eq. (7). Figure 8 shows the

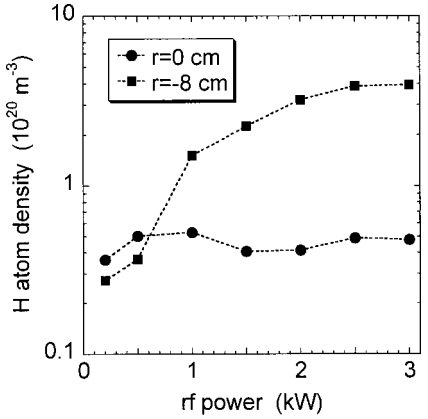

FIG. 8. Absolute H atom density at the center of the plasma column ($r=0$ cm) and at a position 8 cm away from the center of the plasma column ($r=-8$ cm) as a function of the rf power.

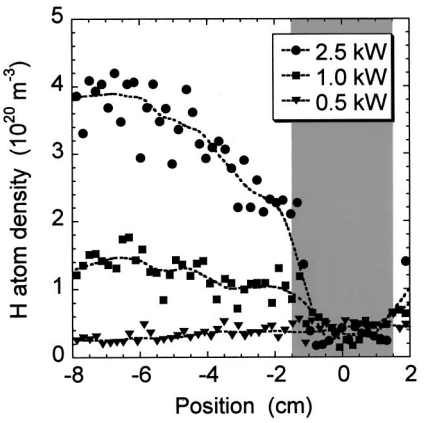

FIG. 9. Radial distribution of the absolute H atom density for rf powers of 0.5, 1.0, and 2.5 kW.

absolute H atom density in H_2 plasmas produced at an H_2 pressure of 30 mTorr. The H atom densities at two different radial positions are plotted. The position $r=0$ cm corresponds to the center of the plasma column, while the position $r=-8$ cm is located 8 cm away from the center of the plasma column. The maximum H atom density of $\sim 4\times10^{14}\,\mathrm{cm}^{-3}$ was observed for a rf power of 3 kW at $r=-8$ cm. Since the pressure of 30 mTorr corresponds to the H_2 density of $1\times10^{15}\,\mathrm{cm}^{-3}$ before the discharge, the maximum H atom density of $\sim 4\times10^{14}\,\mathrm{cm}^{-3}$ means that approximately 20% of the feedstock H_2 dissociated into H atoms. In addition, it can be seen from Fig. 8 that the H atom density in the outside region was higher than that at the center of the plasma column for rf powers higher than 1 kW.

Figure 9 shows spatial (radial) distributions of the H atom density for rf powers of 0.5, 1.0, and 2.5 kW. The gas pressure was 30 mTorr. The spatial distribution was obtained by changing the focus of the laser beam and the observation position of the LIF emission synchronously. In the plasma source used in the present experiment, the plasma column with a diameter of 3 cm was confined radially by the external magnetic field. The shaded region in Fig. 9 represents the location of the plasma column. For a low rf power of 0.5 kW, the radial distribution of the H atom density was roughly uniform, suggesting that the surface loss probability of H is rather small (the chamber walls are located at $r=\pm10$ cm). For an rf power of 1 kW, the H atom density in the plasma column was slightly lower than that in the outside region. For a high rf power of 2.5 kW, a steep gradient was observed at the edge of the plasma column ($r=-1.5$ cm), resulting in the hollow-shaped radial distribution of the H atom density. A possibility for explaining the hollow-shaped density distribution is the distribution of the H atom temperature. However, detailed mechanisms of the hollow-shaped density distribution have not been fully understood yet. Further discussion on the reaction kinetics and transport phenomena in the high-density H_2 plasma is given in a separate paper.[20]

C. Detection limit and the measurement error

The lowest H atom density which can be measured by the present LIF system was approximately $1\times10^{12}\,\mathrm{cm}^{-3}$.

This detection limit is much better than the detection limit of the system developed by Gathen *et al.*[11] The better detection limit was probably obtained by the strong pump laser intensity and the weak stray light. If we replace the detection system with an improved one such as a photon counting system, a very sensitive detection limit could be obtained. In reactive plasmas used for material processing, densities of major radicals are higher than $10^{12}\,\mathrm{cm}^{-3}$. Accordingly, the sensitivity of the present LIF system is high enough to diagnose reactive plasmas used for material processing.

According to Eq. (7), the error in the absolute H atom density evaluated by the present method is estimated by

$$\frac{|\Delta n_{\mathrm{H}}|}{n_{\mathrm{H}}}=\left\{\left(\frac{|\Delta\gamma_r|}{\gamma_r}\right)^2+\left(\frac{|\Delta A_r|}{A_r}\right)^2+\left(\frac{|\Delta N_r|}{N_r}\right)^2+\left(\frac{|\Delta I_r|}{I_r}\right)^2+\left(\frac{|\Delta n_{\mathrm{Xe}}|}{n_{\mathrm{Xe}}}\right)^2\right\}^{1/2}, \tag{8}$$

where $\gamma_r=\gamma_{828}/\gamma_{486}$, $A_r=A_{\mathrm{Xe}}/A_{\mathrm{H}}$, $N_r=\int_0^\infty N_{\mathrm{Xe}}^*(t)dt/\int_0^\infty N_{\mathrm{H}}^*(t)dt$, $I_r=\int_0^\infty I_{\mathrm{H}}(t)dt/\int_0^\infty I_{\mathrm{Xe}}(t)dt$, and the ambiguity in the quantity X is denoted by ΔX. The sensitivity of the detection system at 486 and 828 nm is calibrated using a tungsten standard lamp, and the error is estimated to be $|\Delta\gamma_r|/\gamma_r\simeq 0.2$. The absolute Xe pressure is measured using a capacitance manometer. The accuracy of the absolute Xe pressure depends on the accuracy and the place of the capacitance manometer, and the error is estimated to be $|\Delta n_{\mathrm{Xe}}|/n_{\mathrm{Xe}}\simeq 0.1$. The error in the transition probability is negligibly small in comparison with the errors contained in the other quantities. The ambiguity in the intensity ratio of the LIF emissions from H and Xe is estimated from the run-to-run reproducibility of the signals, and is estimated to be $|\Delta I_r|/I_r\simeq 0.2$. The evaluation of $|\Delta N_r|/N_r$ is difficult since the ambiguities of various parameters used in the rate equations are unknown. However, the close agreement between the experimental results and the rate equation analysis shown in Figs. 5 and 6 suggest a small error in N_r. Here we estimate $|\Delta N_r|/N_r\simeq 0.6$ for the ambiguity in the rate equation analysis. By substituting the above values into Eq. (8), the ambiguity in the absolute H atom density determined by the present method is expected to be less than 70%. This measurement error may be small enough to investigate reaction kinetics of H atoms in reactive plasmas.

ACKNOWLEDGMENT

This work was supported by a Grant-in-Aid for Scientific Research from the Ministry of Education, Science, Sports, and Culture of Japan.

[1] U. Czarnetzki, K. Miyazaki, T. Kajiwara, K. Muraoka, T. Okada, M. Maeda, A. Suzuki, and A. Matsuda, J. Vac. Sci. Technol. A **12**, 831 (1994).
[2] Z. Qing, D. K. Otobaev, G. J. H. Brussaard, M. C. M. van de Sanden, and D. C. Schram, J. Appl. Phys. **80**, 1312 (1996).
[3] J. Cui, Y. Ma, and R. Fang, Appl. Phys. Lett. **69**, 3170 (1996).
[4] K. Tachibana, Jpn. J. Appl. Phys., Part 1 **33**, 4329 (1994).
[5] J. Amorim, J. Loureiro, G. Baravian, and M. Touzeau, J. Appl. Phys. **82**, 2795 (1997).
[6] Y. Kawai, K. Sasaki, and K. Kadota, Jpn. J. Appl. Phys., Part 2 **36**, L1261 (1997).
[7] D. Voslamber, Rev. Sci. Instrum. **71**, 2334 (2000).
[8] D. Voslamber and J. Seidel, Rev. Sci. Instrum. **70**, 928 (1999).
[9] U. Czarnetzki, K. Miyazaki, T. Kajiwara, K. Muraoka, M. Maeda, and H. F. Döbele, J. Opt. Soc. Am. B **11**, 2155 (1994).
[10] A. Goehlich, T. Kawetzki, and H. F. Döbele, J. Chem. Phys. **108**, 9362 (1998).
[11] V. S. von der Gathen, T. Bornrmann, D. Wagner, and H. F. Döbele, Proceedings of the 10th International Symposium on Plasma Chemistry, Bochum, Germany, 1991, Vol. 2, pp. 2.1–2.
[12] K. Miyazaki, T. Kajiwara, K. Uchino, K. Muraoka, T. Okada, and M. Maeda, J. Vac. Sci. Technol. A **14**, 125 (1996).
[13] K. Miyazaki, T. Kajiwara, K. Uchino, K. Muraoka, T. Okada, and M. Maeda, J. Vac. Sci. Technol. A **15**, 149 (1997).
[14] A. Z. Tang, G. J. Salamo, and F. T. Chan, J. Opt. Soc. Am. B **3**, 837 (1986).
[15] A. Brugess, Mem. R. Astron. Soc. **69**, 1 (1965).
[16] W. L. Wiese, M. W. Smith, and B. M. Glennon, *Atomic Transition Probabilities*, Vol. I, Hydrogen through Neon (National Bureau of Standards, Washington, DC, 1966).
[17] S. Kröll and W. K. Bischel, Phys. Rev. A **41**, 1340 (1990).
[18] H. Horiguchi, R. S. F. Chang, and D. W. Steser, J. Chem. Phys. **75**, 1207 (1981).
[19] NIST database, http://physlab.nist.gov.
[20] M. Nakamoto, K. Sasaki, and K. Kadota, Jpn. J. Appl. Phys. (to be published).